Surface plasmon lifetime in metal nanoshells

Arman S. Kirakosyan, Mark I. Stockman, and Tigran V. Shahbazyan

Phys. Rev. B **94**, 155429 — Published 17 October 2016

DOI: 10.1103/PhysRevB.94.155429

Surface Plasmon Lifetime in Metal Nanoshells

Arman S. Kirakosyan,[1] Mark I. Stockman,[2] and Tigran V. Shahbazyan[1*]

[1] *Department of Physics, Jackson State University, Jackson, MS 39217 USA*
[2] *Department of Physics and Astronomy, Georgia State University, Atlanta, GA 30303 USA*

The lifetime of localized surface plasmon plays an important role in many aspects of plasmonics and its applications. In small metal nanostructures, the dominant mechanism of plasmon decay is size-dependent Landau damping. We performed quantum-mechanical calculations of Landau damping for the bright surface plasmon mode in a metal nanoshell with dielectric core. In contrast to the conventional model based on the electron surface scattering, we found that the damping rate decreases as the nanoshell thickness is reduced. The origin of this behavior is traced to the spatial distribution of plasmon local field in the metal shell. We also found that, due to the interference of electron scattering amplitudes from the two nanoshell metal surfaces, the damping rate exhibits pronounced quantum beats with changing shell thickness.

I. INTRODUCTION

Lifetime of localized surface plasmons (SP) in metal nanostructures is one of fundamental problems in plasmonics that has been continuously addressed for about 50 years[1–5]. The importance of this issue stems from one of the major objectives of plasmonics – generation of extremely strong local fields at the nanoscale. The range of physical phenomena and applications related to this goal cuts across physics, chemistry, biology, and device applications. A small sample of examples includes plasmon-enhanced spectroscopies of molecules or semiconductor quantum dots near metal nanostructures, such as surface-enhanced Raman scattering (SERS)[6], plasmon-enhanced fluorescence[7–10], plasmon-assisted fluorescence resonance energy transfer (FRET)[11–14] and plasmonic laser (spaser)[15–20]. High Ohmic losses in bulk metal due to strong electron-phonon interactions impose limitation on the quantum yield of metal-based plasmonic devices, which can, to some extent, be remedied by reducing the metal component size.

However, at the lengthscale below ~ 10 nm, new limitations on the SP lifetime and, consequently, on quantum yield arise due to the quantum-size effects[1]. Among those, the most important is the Landau damping (LD) of SP – decay of SP into the Fermi sea electron-hole pair[21–31]. This process has been recently suggested as an efficient way of hot carriers excitation in plasmon-based photovoltaic devices[32–42]. Starting with the pioneering work of Kawabata and Kubo[43] for a spherical nanoparticle (NP), quantum-mechanical calculations of LD rate were performed, using random phase approximation (RPA)[43–50] or density functional theory (DFT)[51–58] methods, for several NP shapes. Excitation of an electron-hole pair with large optical frequency requires momentum relaxation to satisfy the energy and momentum conservation laws which, in small systems, can take place via the electron surface scattering. Based on this picture, it was suggested[59–63] that the SP LD rate in *any* small system should have the form

$$\gamma_s = A\,\frac{v_F}{L}, \tag{1}$$

where v_F is the electron Fermi velocity (hereafter we set $\hbar = 1$) and L is the effective mean free path of ballistic electrons confined in a hard-wall potential well, while the phenomenological constant A, measured in the range $0.3 - 1.5$[1], accounts for surface potential, electron spillover, and dielectric environment effects. Note that, for nonspherical NPs, the SP damping by interband excitations can complicate the LD size dependence. For example, absorption spectra for gold nanorods[22,27] and nanoshells[23,24] show overall narrowing of the SP resonance that is redshifted away from the interband transitions onset. At the same time, recent systematic studies of scattering spectra of single silver nanoprisms[29], gold nanorods[30], and gold nanodisks[31] revealed significant discrepancies with Eq. (1), while no size-dependence was detected for the SP resonance width of single gold nanoshells[26], implying that LD is shunted by the bulk SP damping even for relatively thin shells.

There is also a physical argument that renders Eq. (1) invalid for nanostructures of general shape. Indeed, the rate of electron-pair excitation by the SP local field must be sensitive to the field distribution in the NP. Note that for a solid sphere, the dipole SP electric field in the NP is uniform and size independent, which is the reason Eq. (1) holds well for spherical NPs in a very wide size range[1]. However, in general case, the local field distribution depends strongly on NP size or shape, so that the simple picture implied by Eq. (1) fails. Below we demonstrate that the effect of field distribution leads to a drastically different size and shape dependence of the LD decay rate in a nanostructure than that implied by Eq. (1).

In this paper, we present a quantum-mechanical calculation of the LD rate for bright SP modes in a metal nanoshell (NS) with a dielectric core. We find that, with decreasing NS thickness d, the LD rate decreases as well, in sharp contrast to the surface scattering model[59–63] predicting an increase of Γ as the effective mean free path is reduced. Furthermore, for small overall NS sizes, the SP LD rate exhibits *quantum beats* as a function of shell thickness caused by the interference between electron scattering amplitudes from the inner and outer NS boundaries.

The paper is organized as follows. In Sec. II we outline our approach and present a formal expression for the LD rate in terms of the SP eigenmodes. In Sec. III we describe the plasmon eigenmodes in metal NS with dielectric core and evaluate the NS internal energy. In Sec. IV, we evaluate the power dissipated through electron-hole excitation by the SP eigenmodes. The calculated LD rates are discussed in Sec. V, and Sec. VI concludes the paper.

II. SURFACE PLASMON LANDAU DAMPING RATE IN COMPOSITE METAL-DIELECTRIC NANOSTRUCTURES

In this section we outline our approach for calculations of the plasmon damping rate in a composite metal-dielectric structure embedded in a dielectric medium. We assume that the structure is characterized by dielectric function of the form $\varepsilon(\omega,\boldsymbol{r})=\varepsilon'(\omega,\boldsymbol{r})+i\varepsilon''(\omega,\boldsymbol{r})$ and the retardation effects are unimportant. In the quasistatic case, the plasmon eigenmodes, labeled by n here, are determined by the Gauss's law

$$\nabla\cdot[\varepsilon'(\omega_n,\mathbf{r})\mathbf{E}_n]=0, \tag{2}$$

where ω_n is the eigenfrequency, $\mathbf{E}_n=-\boldsymbol{\nabla}\Phi_n$ is the mode local field, and Φ_n is the potential. In the following we assume that only the metal dielectric function $\varepsilon_m(\omega)=\varepsilon'_m(\omega)+i\varepsilon''_m(\omega)$ is complex and dispersive. The decay rate of a plasmon mode is given by[64]

$$\Gamma_n=Q_n/U_n, \tag{3}$$

where U_n is the mode energy[65],

$$U_n=\int\frac{dV}{16\pi}\frac{\partial(\omega_n\varepsilon')}{\partial\omega_n}|\mathbf{E}_n|^2=\frac{\omega_n}{16\pi}\frac{\partial\varepsilon'_m}{\partial\omega_n}\int dV_m|\mathbf{E}_n|^2, \tag{4}$$

and Q_n is the mode dissipated power

$$Q_n=\frac{\omega_n}{2}\,\mathrm{Im}\int dV\mathbf{E}_n^*\cdot\mathbf{P}_n, \tag{5}$$

where $\mathbf{P}_n$ is the polarization vector (V_m stands for the metal volume). In the *local* case, i.e., $\mathbf{P}_n=\mathbf{E}_n(\varepsilon-1)/4\pi$, Q is given by the usual expression[65]

$$Q_n=\frac{\omega_n\varepsilon''_m}{8\pi}\int dV_m|\mathbf{E}_n|^2, \tag{6}$$

which, together with the mode energy (4), yields the standard plasmon damping rate[66],

$$\Gamma_n=2\varepsilon''_m\left(\frac{\partial\varepsilon'_m}{\partial\omega_n}\right)^{-1}. \tag{7}$$

For the Drude form of metal dielectric function, $\varepsilon_m=\varepsilon_i-\omega_p^2/\omega(\omega+i\gamma)$, where ε_i is a weakly-dispersive interband contribution, ω_p is the bulk plasmon frequency and γ is the scattering rate, one obtains $\gamma_n=\gamma$ for all modes.

The surface contribution Q_n^s originates from the generation of electron-hole pairs by the plasmon local field near metal-dielectric interfaces, and can be included in Eq. (5) by relating the polarization vector $\mathbf{P}_n(\boldsymbol{r})$ to the microscopic electron polarization operator $P(\omega;\boldsymbol{r},\boldsymbol{r}')$ via the induced charge density: $\rho(\boldsymbol{r})=\int d\boldsymbol{r}'P(\boldsymbol{r},\boldsymbol{r}')\Phi(\boldsymbol{r}')=-\boldsymbol{\nabla}\cdot\mathbf{P}(\boldsymbol{r})$[64]. Integrating Eq. (5) by parts, we obtain

$$Q_n^s=\frac{\omega_n}{2}\,\mathrm{Im}\int dVdV'\Phi_n^*(\boldsymbol{r})P(\omega_n;\boldsymbol{r},\boldsymbol{r}')\Phi_n(\boldsymbol{r}'). \tag{8}$$

In the first-order, Q_n^s is obtained within RPA as[67]

$$Q_n^s=\pi\omega_n\sum_{\alpha\alpha'}|\langle\alpha'|\Phi_n|\alpha\rangle|^2\delta(\epsilon_\alpha-\epsilon_{\alpha'}+\omega_n), \tag{9}$$

where $\langle\alpha'|\Phi_n|\alpha\rangle=\int dV_m\psi^*_{\alpha'}\Phi_n\psi_\alpha$ is the transition matrix element between electron state ψ_α with energy ϵ_α *below* the Fermi level E_F and electron state $\psi_{\alpha'}$ with energy $\epsilon_{\alpha'}$ *above* the Fermi level under the perturbation Φ_n (factor 2 due to the spin degeneracy is included). Note that often in the literature, the plasmon surface-assisted decay rate Γ_n^s is identified with the first-order transition probability rate, similar to Eq. (9) (up to the factor $\omega_n/2$); it must be emphasized that, in a system with dispersive dielectric function, the accurate expression is $\Gamma_n^s=Q_n^s/U_n$[64]. In the rest of this paper, this expression will be used to calculate the SP damping rate in a metal NS.

III. PLASMON MODES IN METAL NANOSHELLS WITH DIELECTRIC CORE

Here we collect the relevant formulas for plasmonic eigenstates in a spherical NS with inner and outer radii R_1 and R_2, respectively, and core dielectric constant ε_c, in a medium with dielectric constant ε_d (see inset in Fig. 1). In the quasistatic limit, the plasmonic eigenfunctions in each region have the form $\Phi_{LM}(\boldsymbol{r})=\Phi_L^{(i)}(r)Y_{LM}(\hat{\boldsymbol{r}})$, where r and $\hat{\boldsymbol{r}}$ are the magnitude and orientation of the radius vector with the origin at NS center, $i=(c,m,d)$ denotes core, metal and outside dielectric regions, respectively, and $Y_{LM}(\hat{\boldsymbol{r}})$ are spherical harmonics. In each region, the eigenfunctions are superpositions of two independent solutions of Laplace equation in spherical coordinates, $r^LY_{LM}(\hat{\boldsymbol{r}})$ and $r^{-L-1}Y_{LM}(\hat{\boldsymbol{r}})$. The equation for eigenvalues is obtained by imposing standard boundary conditions on the radial part of potentials, $\Phi_L^{(i)}(r)$, and radial component of electric field, $E_L^{(i)}(r)=-\partial\Phi_L^{(i)}(r)/\partial r$, as

$$\tilde{\varepsilon}_{cm}\tilde{\varepsilon}_{md}+L(L+1)\varepsilon_{cm}\varepsilon_{md}\kappa^{2L+1}=0, \tag{10}$$

where $\kappa=R_1/R_2$ is the NS aspect ratio, and we denoted $\varepsilon_{\alpha\beta}=\varepsilon'_\alpha-\varepsilon'_\beta$ and $\tilde{\varepsilon}_{\alpha\beta}=L\varepsilon'_\alpha+(L+1)\varepsilon'_\beta$. The plasmon frequencies are obtained by solving Eq. (10) for the real

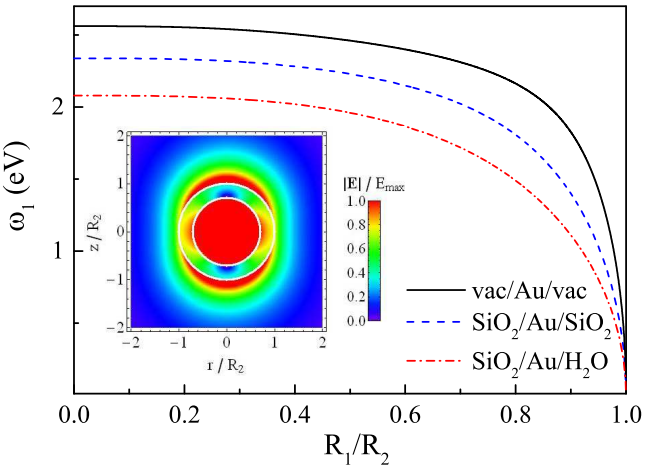

FIG. 1. Frequency of bright dipole plasmon mode in gold NS with various core and outside dielectrics is plotted vs. NS aspect ratio. Inset: Electric field distribution for $SiO_2/Au/H_2O$ NS with aspect ratio $R_1/R_2 = 0.7$.

part of metal dielectric function,

$$\varepsilon'_m(\omega_L) = -\frac{\mu_L}{2} \pm \sqrt{\frac{\mu_L^2}{4} - \varepsilon_c\varepsilon_d},$$
$$\mu_L = \frac{(2L+1)}{L(L+1)}\frac{\tilde{\varepsilon}_{cd}}{(1-\kappa^{2L+1})} - \varepsilon_c - \varepsilon_d, \qquad (11)$$

where alternating ($\pm$) sign correspond to bright and dark plasmon modes, respectively. The bright plasmon spectrum matches that of a solid NP plasmon in the $\kappa = 0$ limit: $\tilde{\varepsilon}_{md} = L\varepsilon'_m + (L+1)\varepsilon_d = 0$. The higher frequency dark plasmon mode couples weakly to the external fields and will not be considered here.

In Fig. 1, we show the dependence of bright plasmon mode frequency ω_1 (for $L = 1$) on aspect ratio $\kappa = R_1/R_2$ of Au NS with several choices of core and outside dielectrics. In all numerical calculations, the experimental dielectric function for gold as well as for core and outside dielectrics were used[68]. With decreasing shell thickness, after a prolonged plateau for κ up to approximately 0.5-0.7 (depending on dielectric content), the frequency develops a redshift. The inset shows electric field distribution for the dipole plasmon mode oscillating along z-axis in a NS with $\kappa = 0.7$. Note that, in a thin NS, the electric field of bright plasmon is mainly concentrated *outside* of the metal shell, in contrast to the field distribution in a solid metal NP.

The normalized (dimensionless) radial eigenfunctions $\Phi_L(r)$ in core ($r < R_1$), shell ($R_1 < r < R_2$), and outer dielectric ($r > R_2$) regions have the form

$$\Phi_L^{(c)}(r) = (2L+1)\frac{\varepsilon'_m\kappa^L}{\tilde{\varepsilon}_{cm}}\left(\frac{r}{R_1}\right)^L, \qquad (12)$$
$$\Phi_L^{(m)}(r) = \kappa^L\left(\frac{r}{R_1}\right)^L + \frac{1}{L+1}\frac{\tilde{\epsilon}_{md}}{\epsilon_{md}}\left(\frac{R_2}{r}\right)^{L+1}, \qquad (13)$$
$$\Phi_L^{(d)}(r) = \frac{2L+1}{L+1}\frac{\varepsilon'_m}{\varepsilon_{md}}\left(\frac{R_2}{r}\right)^{L+1}, \qquad (14)$$

and are continuous at the metal-dielectric interfaces,

$$\Phi_{1L} \equiv \Phi_L^{(m)}(R_1) = (2L+1)\frac{\varepsilon'_m\kappa^L}{\tilde{\varepsilon}_{cm}}, \qquad (15)$$
$$\Phi_{2L} \equiv \Phi_L^{(m)}(R_2) = \frac{2L+1}{L+1}\frac{\varepsilon'_m}{\varepsilon_{md}}. \qquad (16)$$

The radial electric fields satisfy the standard boundary conditions, i.e., $\varepsilon_\alpha E_L^{(\alpha)}(r)$ is continuous, and take the following values at the interfaces (on metal side)

$$E_{1L} \equiv E_L^{(m)}(R_1) = -\frac{L}{R_1}\frac{\varepsilon_c}{\varepsilon'_m}\Phi_{1L},$$
$$E_{2L} \equiv E_L^{(m)}(R_2) = \frac{L+1}{R_2}\frac{\varepsilon_d}{\varepsilon'_m}\Phi_{2L}, \qquad (17)$$

while their ratio at the interfaces is given by

$$q_L = E_{1L}/E_{2L} = -L\kappa^{L-1}\frac{\varepsilon_{md}\varepsilon_c}{\tilde{\varepsilon}_{cm}\varepsilon_d}. \qquad (18)$$

Note that the electric field orientations at the inner and outer interfaces (on the metal side) are opposite.

Using the above eigenfunctions, the plasmon mode energy can be straightforwardly calculated from Eq. (4). Since the eigenfunctions are harmonic functions inside each region, the integral in Eq. (4) reduces to the boundary terms, and, using the relations (17) between fields and potentials at the interface, we obtain

$$U_L = \frac{|\varepsilon'_m|\omega_L}{16\pi}\frac{\partial\varepsilon'_m}{\partial\omega_L}\left[\frac{R_1^3}{L\epsilon_c}E_{1L}^2 + \frac{R_2^3}{(L+1)\epsilon_d}E_{2L}^2\right]. \qquad (19)$$

The aspect ratio dependence of the bright dipole plasmon energy U_1 normalized to solid NP plasmon energy U_1^{np} with the same overall size is plotted in Fig. 2. The NS mode energy depends strongly on core and outside dielectrics, but is largely comparable to that for a solid NP. This is due to a somewhat similar distribution of the surface charges for bright NS plasmon and solid NP plasmon modes: in both cases, the opposite charges are located at different hemispheres so the energy is proportional to the core-shell particle volume. In contrast, for dark modes (not shown here), the opposite charges are located at inner and outer boundaries, so the energy vanishes as the shell thickness decreases.

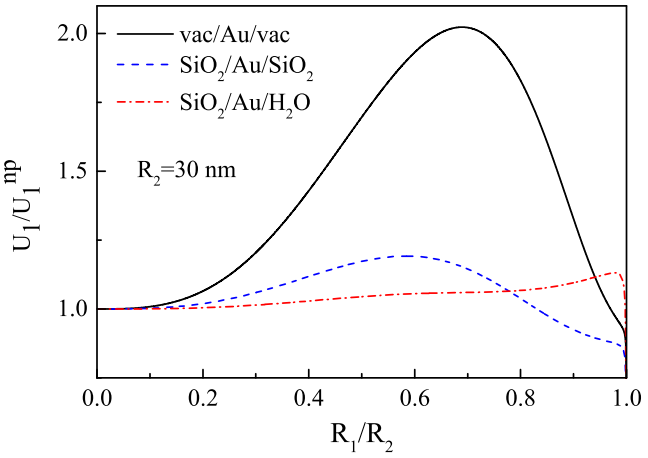

FIG. 2. Normalized energy of bright dipole plasmon modes in gold NS with various core and outside dielectrics is plotted vs. NS aspect ratio.

IV. POWER DISSIPATED BY PLASMON MODES IN NANOSHELLS

We now turn to calculation of dissipated power Eq. (9) (we drop superscript s in the following). We represent NS confining potential as three-dimensional quantum well with hard boundaries at R_1 and R_2 and amplitude V_0: $V(r) = V_0\theta(r-R_1)\theta(R_2-r)$. The role of realistic surface potential and nonlocal effects will be discussed later. The electron wave functions have the form $\psi_{nl}(r)Y_{lm}(\boldsymbol{r})$, where n, l and m and electron radial, angular momentum and magnetic numbers, respectively. Due to spherical symmetry, the angular part factorizes out and Eq. (9) takes the form

$$Q_L = \pi\omega_L \sum_{nn'll'} a^L_{ll'}|M^L_{nl,n'l'}|^2\delta(\epsilon_{nl}-\epsilon_{n'l'}+\omega_L), \quad (20)$$

where $M^L_{nl,n'l'} = \langle nl|\Phi_L|n'l'\rangle$ is radial transition matrix element and

$$a^L_{ll'} = \frac{1}{2L+1}\sum_{Mmm'}\left|\int d\boldsymbol{\Omega} Y_{LM}Y^*_{lm}Y_{l'm'}\right|^2 \quad (21)$$

is the angular contribution. The latter is non-zero only for $l = l' \pm L$, and for typical $l, l' \gg L$, can be approximated as $a^L_{ll'} \approx \delta_{ll'}l/2\pi$.

The matrix element $\langle\alpha|\Phi_{LM}|\alpha'\rangle$ in Eq. (9) is dominated by the surface contribution, which can be obtained by first commuting twice the plasmon potential Φ_{LM} with the Hamiltonian,

$$\langle\alpha|\Phi_{LM}|\alpha'\rangle = \frac{1}{\omega_L^2}\langle\alpha\left[H\left[H,\Phi_{LM}\right]\right]|\alpha'\rangle \approx \frac{1}{m\omega_L^2}\langle\alpha|\nabla\Phi_{LM}\cdot\nabla V|\alpha'\rangle, \quad (22)$$

which, after separating out the angular part, leads to the following expression for the radial matrix element,

$$M^L_{nl,n'l'} = \frac{V_0}{m\omega_L^2}\left[\psi_{nl}(R_1)\psi_{n'l'}(R_1)\mathcal{E}_L(R_1) - \psi_{nl}(R_2)\psi_{n'l'}(R_2)\mathcal{E}_L(R_2)\right]. \quad (23)$$

Then, for infinitely high potential barrier ($V_0 \to \infty$), matching the wave-functions across the well boundaries gives $\sqrt{2mV_0}\psi_{nl}(R_i) \approx -\psi'_{nl}(R_i)$ (here prime stands for the derivative), and the matrix element takes the form

$$M^L_{nl,n'l'} = \frac{1}{2m^2\omega_L^2}\left[\psi'_{nl}(R_1)\psi'_{n'l'}(R_1)E_{1L} - \psi'_{nl}(R_2)\psi'_{n'l'}(R_2)E_{2L}\right]. \quad (24)$$

The first and second terms in the r.h.s. describe excitation, by the plasmon electric field, of a Fermi sea electron-hole pair accompanied by momentum transfer to the inner and outer boundaries, respectively. Correspondingly, Q_L can be decomposed as $Q_L = Q_L^{11} + Q_L^{22} - 2Q_L^{12}$, where

$$Q_L^{ij} = \frac{e^2}{8m^4\omega_L^3}E_{1L}E_{2L} \times\sum_{lnn'}\psi'_{nl}(R_i)\psi'_{n'l}(R_i)\psi'_{nl}(R_j)\psi'_{n'l}(R_j)\delta(\epsilon_{nl}-\epsilon_{n'l}+\omega_L), \quad (25)$$

and we used that $a^L_{ll'} \approx \delta_{ll'}l/2\pi$.

Consider first the inner surface contribution, Q_L^{11}. For typical electron energies $\epsilon_{nl} \sim E_F$, we can adopt semiclassical approximation for the electron wave-functions:

$$\psi_{nl}(r) = \sqrt{\frac{4m}{p_l\tau_l}}\sin\int_r^{R_2} p_l dr,\ p_l = \sqrt{2m\epsilon - \frac{(l+1/2)^2}{r^2}}, \quad (26)$$

where $\tau_l(\epsilon)$ is the period of classical motion between two turning points. In this case, we find

$$\psi'_{nl}(R_1) = -\sqrt{4mp_l(R_1)/\tau_l}. \quad (27)$$

Since the plasmon energy ω_L is much larger than the spacing $\epsilon_0 = v_F/d$ between the energy levels with adjacent n (at fixed l) in a spherical well, the sums in Eq. (25) can be replaced by the integrals, $\sum_n \to \int d\epsilon\rho_l(\epsilon)$ (with $\epsilon < E_F, \epsilon' > E_F$), where $\rho_l(\epsilon) = \partial n/\partial\epsilon_{nl}$ is the partial density of states related to the classical period as $\rho_l = \tau_l/2\pi$ (see Appendix). The result reads

$$Q_L^{11} = \frac{E_{1L}^2}{2\pi^2m^2\omega_L^3}\sum_l l\int_{E_F-\omega_L}^{E_F} d\epsilon p_l(\epsilon,R_1)p_l(\epsilon+\omega_L,R_1). \quad (28)$$

Note that ρ_l cancels out, i.e., the level spacing disappears from the result. In the energy integral, the integration variable is first shifted as $\epsilon \to E_F + \epsilon - \omega_L/2$, where ϵ now changes in the interval $(-\omega_L/2, \omega_L/2)$, and then rescaled to $x = \epsilon/\omega_L$. The sum over l is replaced by the integral restricted by maximal value $l \sim p_F R_1$ that is determined by the condition $p_l(\epsilon, R_1) \geq 0$. After the change of variables to $s = l^2/(p_F R_1)^2$, it contributes a

factor proportional to the inner surface area. The result reads

$$Q_L^{11} = \frac{E_F^2 R_1^2}{2\pi^2 \omega_L^2} E_{1L}^2 \, g\left(\omega/E_F\right), \tag{29}$$

where $g(\xi) = 2\int_{-1/2}^{1/2} dx \int ds f(\xi, x, s)$ with $f(\xi, x, s) = [(1 + \xi x - s)^2 - \xi^2/4]^{1/2}$, is dimensionless function normalized to $g(0) = 1$.

Turning to the outer surface term, Q_L^{22}, the main contribution into the r.h.s. of Eq. (25) comes from the terms with $p_l(\epsilon, R_2) \geq 0$ (otherwise $\psi_{nl}(R_2)$ are exponentially small). In this case, we have

$$\psi'_{nl}(R_2) = -(-1)^n \sqrt{4m p_l(R_2)/\tau_l}, \tag{30}$$

where the sign factor $(-1)^n$ accounts for the *parity* of electron wave-function with $n-1$ nodes between R_1 and R_2. The rest of the calculation is carried in a similar way, and the result,

$$Q_L^{22} = \frac{E_F^2 R_2^2}{2\pi^2 \omega_L^2} E_{2L}^2 \, g(\omega/E_F), \tag{31}$$

is proportional to the outer surface area.

Finally, consider now the interference term Q_L^{12}. Using Eqs. (27) and (30), we write

$$Q_L^{12} = \frac{2E_{1L}E_{2L}}{m^2\omega_L^3} \sum_{lnn'} \frac{l(-1)^{n-n'}}{\tau_l(\epsilon_{nl})\tau_l(\epsilon_{n'l})} \times F_l(\epsilon_{nl}, \epsilon_{n'l}) \delta(\epsilon_{nl} - \epsilon_{n'l} + \omega_L), \tag{32}$$

with $F_l(\epsilon, \epsilon') = \sqrt{p_l(\epsilon, R_1) p_l(\epsilon', R_1) p_l(\epsilon, R_2) p_l(\epsilon', R_2)}$. As ω_L changes (e.g., with changing aspect ratio), the relative parity of electron and hole states, separated by energy ω_L, changes too, leading to a different sequence of alternating signs in the sum in Eq. (32) which, in turn, results in oscillations of Q_L^{12} (quantum beats). The number of states contributing into the sum in Eq. (32) is large, so that the oscillations can be described by substituting $(-1)^{n-n'} = \cos\pi(n-n') = \cos\left[\pi \int_\epsilon^{\epsilon'} d\epsilon \rho_l(\epsilon)\right]$. Then Q_L^{12} takes the form

$$Q_L^{12} = \frac{E_{1L}E_{2L}}{2\pi^2 m^2 \omega_L^3} \sum_l l \int_{E_F - \omega_L}^{E_F} d\epsilon F_l\left(\epsilon, \epsilon + \omega_L\right) \times \cos\left[\pi \int_\epsilon^{\epsilon+\omega_L} d\epsilon' \rho_l(\epsilon')\right], \tag{33}$$

where l is restricted by the condition $p_l(\epsilon, R_1) \geq 0$. Equation (33) can be brought to the form

$$Q_L^{12} = \frac{e^2 R_1^2 E_F^2}{2\pi^2 \omega_L^2} E_{1L} E_{2L} \, G(\omega_L/E_F), \tag{34}$$

where the dimensionless function $G(\xi)$ is rather cumbersome and is given in the Appendix. For thin nanoshels, $d/R_2 \ll 1$, it can be evaluated analytically (see Appendix) and the result reads

$$G(\xi) = -4\frac{\sin D}{D}\frac{\sin(\xi D/4)}{\xi D/4}, \tag{35}$$

where $D = \omega_L/\epsilon_0 = \omega_L d/v_F$ is the ratio of plasmonic and electronic energy scales.

Putting all together, we finally obtain

$$Q_L = \frac{E_F^2 R_2^2}{2\pi^2 \omega_L^2} \left(E_{2L}^2 + \kappa^2 E_{1L}^2 - 2\kappa^2 E_{1L} E_{2L} G\right). \tag{36}$$

The last term in Q_{12} oscillates as a function of shell thickness d due to the interference of electron scattering amplitudes from inner and outer NS boundaries. These oscillations are, in fact, *quantum beats* caused by the change, with d, of the number of electron levels with alternating parities within the plasmon energy ω_L (i.e., the difference between numbers of even and odd states oscillates between 0 and 1). The oscillations period $2\pi v_F/\omega_L$ depends weakly on the shell thickness through dependence of ω_L on κ (see Fig. 1), and their amplitude slowly dies out with increasing d.

In fact, the quantum beats of Q_{12} have a rather general origin. Indeed, excitation of an electron-hole pair with energy ω is accompanied by momentum transfer $p_0 \sim \omega/v_F$ and occurs in a region with the size $r_0 \sim v_F/\omega$. Therefore, oscillations of the pair excitation rate with changing $D = d/r_0$ reflect the nonlocality of surface-scattering mechanism of momentum relaxation.

In Fig. 3, normalized dissipated power for the bright dipole plasmon mode Q_1 is plotted vs. aspect ratio κ for overall NS sizes $R_2 = 30$ nm and $R_2 = 10$ nm. Numerical calculations were performed using the full expression for $G(\xi)$ given by Eq. (A.1) in the Appendix. While for larger NS with overall size $R_2 = 30$ nm, oscillations of Q_1 are relatively weak [see Fig. 3(a)], they become more pronounced for smaller NS ($R_2 = 10$ nm) [see Fig. 3(b)]. Note that, for smaller R_2, same values of κ correspond to smaller shell thicknesses. Another striking feature is the *decrease* of dissipated power for κ larger than 0.4. The reason for this behavior is that, with decreasing shell thickness, the local field is pushed outside the metal shell (see inset in Fig. 1) which, in turn, leads to the reduction of the transition matrix element.

V. LANDAU DAMPING OF PLASMON MODES IN NANOSHELLS

The plasmon damping rate, $\Gamma_L = Q_L/U_L$ with Q_L and U_L given by Eqs. (36) and (19), respectively, takes the form

$$\Gamma_L = \frac{2\omega_p^2 \gamma_L}{\omega_L^3} \left(\frac{\partial \varepsilon'_m}{\partial \omega_n}\right)^{-1}, \tag{37}$$

where

$$\gamma_L = \frac{3v_F}{4R_2} \frac{\varepsilon_d(L+1)}{|\varepsilon'_m(\omega_L)|} \frac{1 + \kappa^2 q_L^2 - 2\kappa^2 q_L G}{1 + \kappa^3 q_L^2 (L+1)\varepsilon_d/L\varepsilon_c} \tag{38}$$

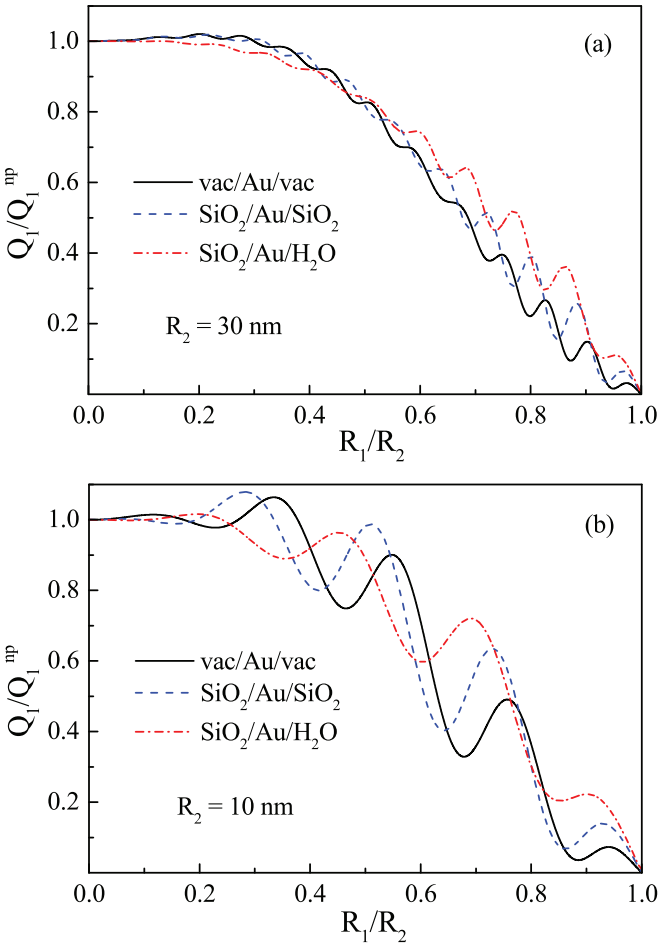

FIG. 3. Normalized dissipated power by bright dipole plasmon modes in gold NS with various core and outside dielectrics is plotted vs. NS aspect ratio for (a) $R_2 = 30$ nm and (b) $R_2 = 10$ nm.

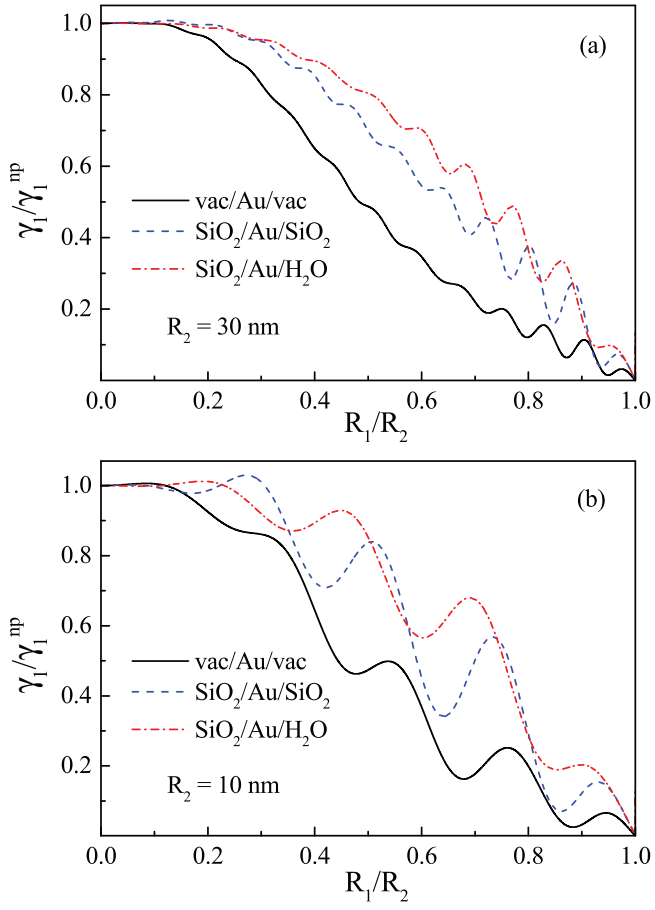

FIG. 4. Normalized Landau damping rate for bright dipole plasmon modes in gold NS with various core and outside dielectrics is plotted vs. NS aspect ratio for (a) $R_2 = 30$ nm and (b) $R_2 = 10$ nm.

is the LD rate. Here $q_L = E_{1L}/E_{2L}$ is the electric fields' ratio at the interfaces given by Eq. (18). In deriving Eq. (38), we used the relation $\omega_p^2 = 4\pi n/m = 4p_F^3/3\pi m$ (for $e = 1$), where n is the electron concentration.

Equations (37) and (38) represent our central result. Apart from the dimensional factor v_F/R_2, the LD rate (38) is determined by the ratio of plasmon local fields at the metal-dielectric interfaces q_L. The last factor describes the relative contribution of the NS interfaces and includes the interference correction. Importantly, comparison of Eqs. (37) and (7) indicates that LD rate can be incorporated into the Drude scattering rate as $\gamma = \gamma_0 + \gamma_L$, where γ_0 is the bulk scattering rate, so the full plasmon damping rate is still given by Eq. (7), but with modified Drude dielectric function.

For solid NP ($\kappa = 0$), the plasmon eigenfrequency is determined from $L\varepsilon_m(\omega_L)+(L+1)\varepsilon_d = 0$, and we recover the LD rate of the Lth mode in a spherical NP[43–47],

$$\gamma_L^{np} = \frac{3L}{4}\frac{v_F}{R_2}. \qquad (39)$$

In thin NSs, the electric field is pushed out of the metal shell, leading to the reduction of electron-hole excitation rate. For thin NS ($d/R_2 \ll 1$), the explicit dependence of the LD rate on the shell thickness is obtained from Eq. (38) as (for $L = 1$)

$$\gamma_1 \approx \frac{3}{2}\frac{v_F d}{R_2^2}\left[1 - \frac{4\varepsilon_c\varepsilon_d}{\tilde{\varepsilon}_{cd}^2}(1-G)\right], \qquad (40)$$

indicating a *linear* dependence on the shell thickness.

In Fig. 4, we show the calculated LD rate γ_1 for the bright dipole plasmon mode in gold NSs of overall sizes $R_2 = 30$ nm and $R_2 = 10$ nm and several choices of core and outside dielectrics. The rate shows approximately linear decrease with increasing κ (i.e., decreasing d), consistent with Eq. (40). The oscillations of γ_1 are quite pronounced for smaller overall NS size ($R_2 = 10$ nm) and could be observable for typical experimental range of aspect ratios (0.6-0.8) provided that NS overall size is sufficiently small, so that the LD is not shunted by the bulk scattering. Note that these oscillations should be distinguished from those observed in solid NP[51,52,57] due to size-quantization of the electron energy levels in

a confined nanostructure, while here they are quantum beats between electron scattering paths from different NS interfaces.

VI. CONCLUSIONS

In conclusion, let us discuss the role surface potential, dielectric environment and nonlocal effects near the metal surface on the plasmon LD that was extensively studied in solid NPs[51–58]. These effects mainly affects the overall magnitude of LD rates, but plays no significant role in determining the LD dependence on the nanostructure shape which, according to our findings, is mainly determined by the local field ratio at the interfaces. Extensive theoretical and experimental studies of spherical NPs indicate that surface effects mainly affect the phenomenological constant A [see Eq. (1)], but the overall $1/R$ dependence of the LD rate is unchanged[1]. In fact, the important role of local fields in plasmon LD rate can explain the relatively wide range of measured A (0.3-1.5[1]), which raised questions about the validity of scattering model[56]. Indeed, as we mentioned in Sec. IV, excitation of an e-h pair by plasmon local field takes place in a surface layer of thickness $r_0 \sim v_F/\omega$. For $v_F \approx 1.4\times10^6$ m/s in Au and Ag, we have $v_F/\omega \approx 1$ nm for $\hbar\omega = 1.0$ eV, i.e., for typical plasmon frequencies in the range 1.5-3.5 eV, the layer thickness is just a few Å. In a thin surface layer, the local fields are strongly affected by the electron spillover and surface roughness effects as well as by the dielectric environment, which can lead to large variations of overall LD rate magnitude for different samples and/or environments. Within our approach, the constant A can be estimated by computing the effect of the above factors on the local field, which is, however, out of scope of this paper.

In summary, we calculated the Landau damping rate of surface plasmons in metal nanoshells with dielectric core. We found that the damping rate decreases with the shell thickness due to the reduction of the local field magnitude inside a thin metal shell. We also found that the Landau damping rate exhibits quantum beats caused by the interference between electron scattering paths from the nanoshell inner and outer metal-dielectric interfaces.

ACKNOWLEDGMENTS

This work was supported in part by NSF Grants No. DMR-1610427 and No. HRD-1547754.

Appendix

Here we analyze function $G(\xi)$ in the interference term (34). After shifting integration variables in Eq. (33) as $\epsilon \to E_F + \epsilon - \omega_L/2$ and $\epsilon' \to E_F + \epsilon + \epsilon'$ and rescaling to $x = \epsilon/\omega_L$ and $s = l^2/(p_F R_1)^2$, we arrive at (34) with

$$G(\xi) = 2\int_{-1/2}^{1/2} dx \int ds \sqrt{f(\xi,x,s)f(\xi,x,\kappa^2 s)} \times \cos\left[\pi\omega_L \int_{-1/2}^{1/2} dx' \rho_l\big[E_F[1+\xi(x+x')]\big]\right], \quad \text{(A.1)}$$

where $f(\xi,x,s) = \sqrt{(1+\xi x - s)^2 - \xi^2/4}$, and the partial density of states is given by

$$\rho_l(\epsilon) = \frac{m}{\pi}\int_{R_1}^{R_2}\frac{dr}{p_l(\epsilon,r)} = \frac{R_2 p_l(\epsilon,R_2) - R_1 p_l(\epsilon,R_1)}{2\pi\epsilon} \quad \text{(A.2)}$$

$$= \frac{R_2}{\pi v_F}\left[\frac{\sqrt{1+\xi(x+x')-\kappa^2 s} - \kappa\sqrt{1+\xi(x+x')-s}}{1+\xi(x+x')}\right].$$

For $\omega/E_F \ll 1$, the x'-integrals are easily evaluated, yielding

$$G(\xi) = 2\int_{-1/2}^{1/2} dx \int_0^{1+\xi x} ds \sqrt{f(\xi,x,s)f(\xi,x,\kappa^2 s)} \times \cos\left[w(\xi,x,s)\omega_L/\epsilon_0\right], \quad \text{(A.3)}$$

where $w(\xi,x,s) = \left(\sqrt{f(\xi,x,\kappa^2 s)} - \kappa\sqrt{f(\xi,x,s)}\right)/(1+\xi x)$ with $f(\xi,x,s) \approx 1+\xi x - s$ (here $\epsilon_0 = v_F/R_2$). Rescaling s by $1+\xi x$, Eq. (A.3) factorizes as $G(\xi) = \int_{-1/2}^{1/2} dx\,(1+\xi x)^2\, S(\xi,x)$, where

$$S(\xi,x) = 2\int_0^1 ds\sqrt{(1-s)(1-\kappa^2 s)} \times \cos\left[a(\xi,x)\left(\sqrt{1-\kappa^2 s} - \kappa\sqrt{1-s}\right)\right], \quad \text{(A.4)}$$

with shorthand notation $a(\xi,x) = (\omega_L/\epsilon_0)/\sqrt{1+\xi x}$. With substitution $s = 1 - \frac{1-\kappa^2}{\kappa^2}\sinh^2\alpha$, S is brought to the form

$$S(\xi,x) = \frac{4(1-\kappa^2)^2}{\kappa^3}\int_0^{\alpha_0} d\alpha\,(\sinh\alpha\cosh\alpha)^2 \times \cos\left[a(\xi,x)\sqrt{1-\kappa^2}e^{-\alpha}\right], \quad \text{(A.5)}$$

where $\sinh\alpha_0 = \kappa/\sqrt{1-\kappa^2}$. For $a(\xi,x) \gg 1$, the integral is dominated by the upper limit, and for thin shells, $1-\kappa \ll 1$, corresponding to $\alpha_0 > 1$, can be evaluated as

$$S \approx -4\frac{\sin(a\sqrt{1-\kappa^2}e^{-\alpha_0})}{a\sqrt{1-\kappa^2}e^{-\alpha_0}} = -4\frac{\sin\left[a(1-\kappa)\right]}{a(1-\kappa)}. \quad \text{(A.6)}$$

With the above S and after change of variable $t = \sqrt{1+\xi x}$, the expression for $G(\xi)$ takes the form

$$G(\xi) = -\frac{8}{\xi D}\int_{t_-}^{t_+} dt t^3 \sin(tD), \quad \text{(A.7)}$$

where $t_\pm = \sqrt{1 \pm \xi/2}$, and $D = (1-\kappa)\omega_L/\epsilon_0 = \omega_L d/v_F$. Note that even though for $\xi \ll 1$ the integration interval is small, the integrand is still an oscillating function since $D \gg 1$ and so the product $D\xi$ can be arbitrary. In this case, a straightforward evaluation yields Eq. (35).

* shahbazyan@jsums.edu

[1] U. Kreibig and M. Vollmer, *Optical Properties of Metal Clusters* (Springer, Berlin, 1995).
[2] W. P. Halperin, Rev. Mod. Phys. **58**, 533 (1986).
[3] V. V. Kresin, Phys. Rep. **220**, 1 (1992).
[4] K. L. Kelly, E. Coronado, L. L. Zhao, G. C. Schatz, J. Phys. Chem. B **107**, 668 (2003).
[5] C. Noguez, J. Phys. Chem. C **111** 3806 (2007).
[6] E. C. Le Ru and P. G. Etchegoin, *Principles of Surface-Enhanced Raman Spectroscopy* (Elsevier, 2009).
[7] E. Dulkeith, A. C. Morteani, T. Niedereichholz, T. A. Klar, J. Feldmann, S. A. Levi, F. C. J. M.. van Veggel, D. N. Reinhoudt, M. Moller, and D. I. Gittins, Phys. Rev. Lett. **89**, 203002 (2002).
[8] P. Anger, P. Bharadwaj, and L. Novotny, Phys. Rev. Lett. **96**, 113002 (2006).
[9] S. Kühn, U. Hakanson, L. Rogobete, and V. Sandoghdar, Phys. Rev. Lett. **97**, 017402 (2006).
[10] F. Tam, G. P. Goodrich, B. R. Johnson, and N. J. Halas, Nano Lett. **7**, 496 (2007).
[11] J. R. Lakowicz, J. Kusba, Y. Shen, J. Malicka, S. DAuria, Z. Gryczynski, I. Gryczynski, J. Fluoresc. **13**, 69 (2003).
[12] P. Andrew and W. L. Barnes, Science **306**, 1002 (2004).
[13] F. Reil, U. Hohenester, J. R. Krenn, and A. Leitner, Nano Lett. 8, 4128 (2008).
[14] M. Lunz, V. A. Gerard, Y. K. Gunko, V. Lesnyak, N. Gaponik, A. S. Susha, A. L. Rogach, and A. L. Bradley, Nano Lett. **11**, 3341 (2011).
[15] D. J. Bergman and M. I. Stockman, Phys. Rev. Lett., **90**, 027402, (2003).
[16] M. I. Stockman, Nature Photon. **2**, 327, (2008).
[17] M. A. Noginov, G. Zhu, A. M. Belgrave, R. Bakker, V. M. Shalaev, E. E. Narimanov, S. Stout, E. Herz, T. Suteewong and U. Wiesner, Nature, **460**, 1110, (2009).
[18] R. F. Oulton, V. J. Sorger, T. Zentgraf, R.-M. Ma, C. Gladden, L. Dai, G. Bartal, and X. Zhang, Nature **461**, 629, (2009).
[19] Y.-J. Lu, J. Kim, H.-Y. Chen, C.i Wu, N. Dabidian, C. E. Sanders, C.-Y. Wang, M.-Y. Lu, B.-H. Li, X. Qiu, W.-H. Chang, L.-J. Chen, G. Shvets, C.-K. Shih, and S. Gwo, Science **337**, 450 (2012).
[20] A. Yang, T. B. Hoang, M. Dridi, C. Deeb, M. H. Mikkelsen, G. C. Schatz, and T. W. Odom, Nature Comm. **6**, 6939 (2015).
[21] T. Klar, M. Perner, S. Grosse, G. von Plessen, W. Spirkl, and J. Feldmann, Phys. Rev. Lett. **80**, 4249 (1998).
[22] C. Sönnichsen, T. Franzl, T. Wilk, G. von Plessen, J. Feldmann, O. V. Wilson, and P. Mulvaney, Phys. Rev. Lett. **88**, 077402 (2002).
[23] S. L. Westcott, J. B. Jackson, C. Radloff, and N. J. Halas, Phys. Rev. B **66**, 155431 (2002).
[24] G. Raschke, S. Brogl, A. S. Susha, A. L. Rogach, T. A Klar, and J. Feldmann, Nano Lett. **4**, 1853 (2004).
[25] A. Arbouet, D. Christofilos, N. Del Fatti, F. Vallëe, J. R. Huntzinger, L. Arnaud, P. Billaud, and M. Broyer, Phys. Rev. Lett. **93**, 127401 (2004).
[26] C. L. Nehl, N. K. Grady, G. P. Goodrich, F. Tam, N. J. Halas, and J. H. Hafner, Nano Lett. **4**, 2355 (2004).
[27] C. Novo, D. Gomez, J. Perez-Juste, Z. Zhang, H.Petrova, M. Reismann, P. Mulvaney, and G. V. Hartland, Phys. Chem. Chem. Phys. **8**, 3540 (2006)
[28] H. Baida, P. Billaud, S. Marhaba, D. Christofilos, E. Cottancin, A. Crut, J. Lermé, P. Maioli, M. Pellarin, M. Broyer, N. Del Fatti, and F. Vallée, Nano Lett. **9**, 3463 (2009).
[29] M. G. Blaber, A.-I. Henry, J. M. Bingham, G. C. Schatz, and R. P. Van Duyne, J. Phys. Chem. C **116**, 393 (2012).
[30] V. Juvé, M. F. Cardinal, A. Lombardi, A. Crut, P. Maioli, J. Përez-Juste, L. M. Liz-Marzán, N. Del Fatti, and F. Vallée, Nano Lett. **13**, 2234 (2013).
[31] M. N. O'Brien, M. R. Jones, K. L. Kohlstedt, G. C. Schatz, and C. A. Mirkin, Nano Lett. **15**, 1012 (2015).
[32] Y. K. Lee, C. H. Jung, J.Park, H. Seo, G. A. Somorjai, and J. Y. Park, Nano Lett. **11**, 4251 (2011).
[33] F. Wang, N. A. Melosh, Nano Lett. **11**, 5426 (2011).
[34] A. Sobhani, M. W. Knight, Y. Wang, B. Zheng, N. S. King, L. V. Brown, Z. Fang, P. Nordlander, and N. J. Halas, Nat. Commun. **4**, 1643 (2013).
[35] A. Hoggard, L.-Y. Wang, L. Ma, Y. Fang, G. You, J. Olson, Z. Liu, W.-S. Chang, P. M. Ajayan, and S. Link, ACS Nano **7**, 11209 (2013).
[36] K. Wu, W. E. Rodriguez-Cordoba, Y. Yang, and T. Lian, Nano Lett. **13**, 5255 (2013).
[37] A. Giugni, B. Torre, A. Toma, M. Francardi, M. Malerba, A. Alabastri, R. P. Zaccaria, M. I. Stockman, and E. Di Fabrizio, Nat. Nanotechnol. **8**, 845 (2013).
[38] C. Clavero, Nat. Phot. **8**, 95 (2014).
[39] H. Chalabi, D. Schoen, M. L. Brongersma, Nano Lett. **14**, 1374 (2014).
[40] B. Y. Zheng, H. Zhao, A. Manjavacas, M. McClain, P. Nordlander, and N. J. Halas, Nat. Commun. **6**, 7797 (2015).
[41] J. Ma, Z. Wang, and L.-W. Wang, Nat. Commun. **6**, 10107 (2015).
[42] M. L. Brongersma, N. J. Halas, and P. Nordlander, Nat. Nanotechnol. **10**, 25 (2015).
[43] A. Kawabata and R. Kubo, J. Phys. Soc. Jpn. **21**, 1765 (1966).
[44] A. A. Lushnikov and A. J. Simonov, Z. Physik **270**, 17 (1974).
[45] W. A. Kraus and G. C. Schatz, J. Chem. Phys. **79**, 6130 (1983).
[46] M. Barma and V. J. Subrahmanyam, J. Phys.: Cond. Mat. **1**, 7681 (1989).
[47] C. Yannouleas and R. A. Broglia, Ann. Phys. **217**, 105 (1992).
[48] M. Eto and K. Kawamura, Surf. Rev. Lett. **03**, 151 (1996).
[49] A. V. Uskov, I. E. Protsenko, N. A. Mortensen, and E. P. OReilly, Plasmonics **9**, 185 (2013).
[50] J. B. Khurgin and G. Sun, Opt. Exp. **23**, 250905 (2015).
[51] R. A. Molina, D. Weinmann, and R. A. Jalabert, Phys. Rev. B **65**, 155427 (2002).

[52] G. Weick, R. A. Molina, D. Weinmann, and R. A. Jalabert, Phys. Rev. B **72**, 115410 (2005).
[53] Z. Yuan and S. Gao, Surf. Sci. **602**, 440 (2008).
[54] J. Lermé, H. Baida, C. Bonnet, M. Broyer, E. Cottancin, A. Crut, P. Maioli, N. Del Fatti, F. Vallée, and M. Pellarin, J. Phys. Chem. Lett. **1**, 2922 (2010).
[55] J. Lermé, J. Phys. Chem. C **115**, 14098 (2011).
[56] J. A. Scholl, A. L. Koh, J. A. Dionne, Nature **483**, 421 (2012).
[57] X. Li, Di Xiao, and Z. Zhang, New J. Phys. **15**, 023011 (2013).
[58] A. Manjavacas, J. G. Liu, V. Kulkarni, and P. Nordlander, ACS Nano **8**, 7630 (2014).
[59] L. Genzel, T. P. Martin, and U. Kreibig, Z. Phys. B **21**, 339 (1975).
[60] R. Ruppin and H. Yatom, Phys. Status Solidi **74**, 647 (1976).
[61] W. A. Krauss and G. C. Schatz, Chem. Phys. Lett. **99**, 353 (1983).
[62] E. A. Coronado and G. C. Schatz, J. Chem. Phys. **119**, 3926 (2003).
[63] A. Moroz, J. Phys. Chem. C **112**, 10641 (2008).
[64] T. V. Shahbazyan, arXiv:1602.05977.
[65] L. D. Landau and E. M. Lifshitz, *Electrodynamics of Continuous Media* (Elsevier, Amsterdam, 2004).
[66] M. I. Stockman, *Nanoplasmonics: From Present into Future*, in *Plasmonics: Theory and Applications*, edited by T. V. Shahbazyan and M. I. Stockman (Springer, New York, 2013).
[67] G.D. Mahan, *Many-Particle Physics* (Plenum, New York, 1990).
[68] P. G. Etchegoin, E. C. Le Ru, and M. Meyer, J. Chem. Phys. **125**, 164705 (2006).